JOURNAL OF SPACECRAFT AND ROCKETS
Vol. 37, No. 1, January–February 2000

Engineering Notes

ENGINEERING NOTES are short manuscripts describing new developments or important results of a preliminary nature. These Notes cannot exceed 6 manuscript pages and 3 figures; a page of text may be substituted for a figure and vice versa. After informal review by the editors, they may be published within a few months of the date of receipt. Style requirements are the same as for regular contributions (see inside back cover).

Forebody Convective Hypersonic Heat Transfer Measurements over Large-Angle Blunt Cones

G. Jagadeesh,* N. M. Reddy,† K. Nagashetty,‡
and K. P. J. Reddy§
Indian Institute of Science, Bangalore 560 012, India

Introduction

KNOWLEDGE of surface heat transfer rates for a vehicle configuration under hypersonic flow is essential to quantify the heat-shielding requirement for the thermal protection system (TPS) of space missions. Typically low-lift and high-drag bodies such as large-angle blunt cones are used as heat shields in modern aero-assisted orbital transfer vehicles[1] (AOTVs). The development of these space vehicles requires a large volume of heat transfer data, which can also be used to validate computational fluid dynamic codes. Although most of the AOTVs operate at very high velocities and high altitudes, the maximum convective heating will occur at conditions corresponding to continuum/near-continuum flow.[2] Hence, carefully designed ground-based experiments in typical high enthalpy continuum flow conditions will be very useful in designing the requisite TPS for such space missions. Previously, many authors have reported heat transfer measurements over large-angle blunt bodies.[3–5]

In this Note we report the development of useful heat transfer correlations that are independent of the angle of attack, for 60-deg half-angle blunt cones at a nominal Mach number of 5.75. These correlations are based on heat transfer measurements in the Indian Institute of Science hypersonic shock tunnel-HST1 (Ref. 6) with both air and carbon dioxide as test gases. These measurements include the effects of stagnation enthalpy, test gas, corner bluntness, and angle of attack on the surface heat transfer distributions over the model. The experimental results are also compared with axisymmetric Navier–Stokes (N–S) solutions at 0-deg angle of attack.

Results and Discussion

The measurements are made at a freestream Mach number of 5.75 and unit Reynolds numbers 1.438×10^6 and 1.965×10^6 using air and helium driver gases, respectively (Table 1). The test models are a 120-deg blunt cone with a sharp corner and another with a corner radius. Platinum thin-film sensors deposited on Macor® substrates have been used for heat transfer measurements.[7] Based on the uncertainties associated with the gauge characteristics, circuitry, data acquisition system, calibration, and data-reduction procedure, the measured values of heat transfer rates are believed to be accurate to ±5% for high-enthalpy tests (helium as driver gas) and ±11% for low-enthalpy tests (air as the driver gas), as a conservative estimate.

The experimental heating rates on the blunt cone model correspond to the vertical ray expressed in terms of the wetted surface length, s/R_n, measured from the geometric stagnation point at zero incidence. These measurements show that the surface heating rates in the stagnation zone of the blunt cone increased fivefold when the stagnation enthalpy H_0 is doubled. Typically, at $H_0 = 0.68$ MJ/kg, the measured heat transfer in the stagnation point is ~6.5 W/cm^2 whereas the heating rate increases to ~30 W/cm^2 at $H_0 = 1.2$ MJ/kg. This is essentially due to the large kinetic energy dissipation of the flow in the thin shock layer at higher freestream velocities. Although the enhanced heat transfer is obvious from the increased kinetic energy dissipation at higher enthalpies, the precise quantification of these enhanced heat transfer rates presented here are very useful. At zero angle of incidence, the corner heating increases by 20–30% of the stagnation point heat transfer at $H_0 = 1.2$ MJ/kg, whereas it increases by 30–40% at $H_0 = 0.68$ MJ/kg. The variation of surface Stanton number St at different angles of attack for the blunt cone with sharp corner is shown in Fig. 1. The Stanton number is defined as $St = q(t)/\{\rho_\infty V_\infty (H_{0w} - H_w)\}$, where $q(t)$ is the heat transfer rate, ρ_∞ is the freestream density, V_∞ is the freestream velocity of the flow, H_{0w} is the stagnation enthalpy, and H_w is the enthalpy at the wall. Increased windward heating and increased corner heating with increase in angle of attack are observed as reported previously.[3–5]

To evaluate the effect of test gas on the heat transfer distributions on the blunt cones, experiments have been carried out using carbon dioxide as the test gas. The shock wave will be relatively closer to the body in carbon dioxide environment compared to air. About 15–20% increase in the measured heating rates in carbon dioxide environment has been observed compared to air as the test gas. Similar results have been reported[4] previously for a 140-deg blunt cone. Thus, this study indicates that the large-angle blunt cone when used as aerobrake in Martian atmosphere would encounter slightly

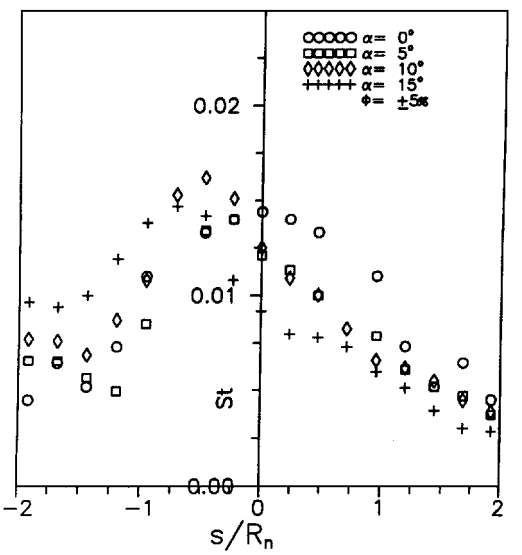

Fig. 1 Variation of Stanton number at different angles of attack on blunt cone model with sharp corner: H_0 = 1.2 MJ/kg.

Presented as Paper 98-2601 at the AIAA 20th Advanced Measurement and Ground Testing Technology Conference, Albuquerque, NM, 15–18 June 1998; received 10 October 1998; revision received 7 October 1999; accepted for publication 7 October 1999.

*Research Scholar, Department of Aerospace Engineering.
†Emeritus Professor, Department of Aerospace Engineering. Associate Fellow AIAA.
‡Junior Scientific Assistant, Department of Aerospace Engineering. Member AIAA.
§Associate Professor, Department of Aerospace Engineering.

Table 1 Nominal flow conditions for the heat transfer experiments

Driver gas	H_0,[a] MJ/kg	P_0, kN/m^2	T_0, K	U_∞,[b] m/s	T_∞, K	ρ_∞, kg/m^3	P_∞, kN/m^2	M_∞	Re, m^{-1}	Q_0,[c] W/cm^2
Air	0.6862	254.85	683.179	1092.03	89.76	0.0081	209.39	5.75	1.438×10^6	6.78
Helium	1.215	811.13	1209.56	1453.06	158.9	0.0146	666.4	5.75	1.965×10^6	28.7

[a]Subscript 0 indicates reservoir condition. [b]Subscript ∞ indicates freestream condition. [c]Stagnation point heating rate.

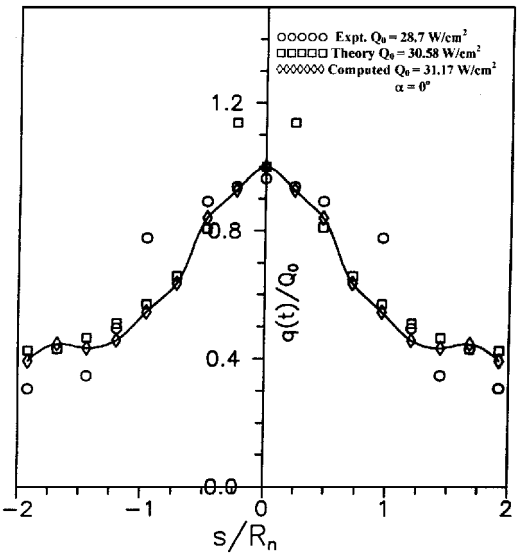

Fig. 2 Comparative convective heating rates for blunt cone with sharp corner.

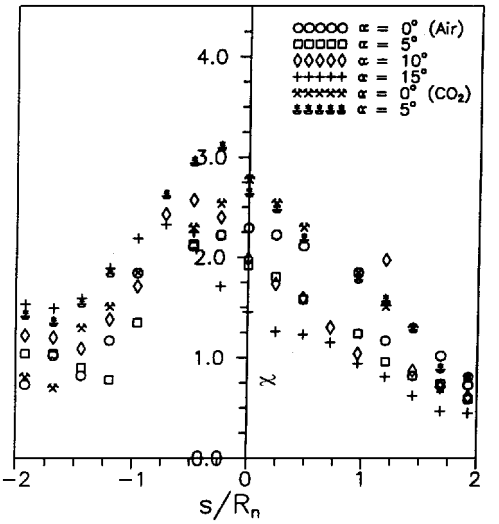

Fig. 3 Heat transfer correlation for blunt cone with blunt corner: H_0 = 1.2 MJ/kg.

higher aerodynamic heating due to the presence of carbon dioxide in the atmosphere.

The experimental results have also been compared with the axisymmetric N–S computations using the three-dimensional N–S solver CFX TASCflow (AEA Technology, plc, United Kingdom) for large-angle blunt cone with a sharp corner at zero angle of incidence. In this analysis no-slip wall boundary conditions are assumed at a constant wall temperature of 298 K, and the radiative component of heat transfer is neglected in the computations. The computed surface heating rates along with both experimental and theoretical estimates are shown in Fig. 2. It is seen that the measured values match within ±9% with the computed values.

The viscous effects and the entropy swallowing effects are some of the very distinct features of hypersonic flow regime. Reduced shock detachment distance around the blunt cones at high Mach numbers due to the higher density ratio across the shock waves result in a faster swallowing effect of the entropy gradients. Overall, one can identify two important phenomena that influence the heat transfer. First, the curved shock around the blunt nose produces an entropy layer that interacts with boundary layer that in turn increases the surface heating. Second, the viscous interaction between the thick hypersonic boundary layer around the blunt cone and the outer inviscid flow is quite significant. Compared to the inviscid case, this leads to very strong pressure decrease, which also produces higher surface heating in the downstream direction. Hence, the heat transfer measurements have been correlated in terms of the viscous interaction parameter and the shock density ratio, yielding $\chi = St(\rho_2/\rho_\infty)^{2/3}/M_\infty (C^*/Re_{\infty n})^{0.5}$, where $Re_{\infty n}$ is the Reynolds number based on the nose radius of the blunt cone model, C^* is the Chapman–Rusbin factor given by $(\mu^* T_\infty/\mu_\infty T^*)$, and μ^* is the reference viscosity calculated at the reference temperature in degrees Kelvin $T^* = (T_{02}/6)(1 + 3T_w/T_{02})$. The starred quantities are the reference values, and the subscripts w and 02 indicate the wall and the stagnation conditions, respectively. This approach is based on the work by Cheng et al.[8] The exponent of the density ratio, which is attributed to the bluntness effect, depends on the geometry and the flow conditions. It is observed that the heat transfer measurements irrespective of the angle of incidence correlate very well when expressed in terms of χ.

The heat transfer correlation for the blunt cone model with blunt corner at high-enthalpy condition is shown Fig. 3. Slightly higher corner heating peaks are observed in these plots for air as test gas compared to carbon dioxide. Similarly, slightly higher values of the correlation parameter are observed in the low-enthalpy condition compared to high-enthalpy conditions. However, this correlation does not encompass all of the physics and chemistry of the flow conditions. Moreover, there appears to be a greater sensitivity of heat transfer to γ, but it is very difficult to justify the slight differences seen in the correlated heat transfer distributions for carbon dioxide compared to air as the test gas. This correlation is very significant in the sense that the surface heat transfer distributions for large-angle blunt cones depend mainly on the viscous interaction parameter and the entropy swallowing effect.

Conclusion

We have presented the forebody surface convective heat transfer rates over large-angle blunt cones measured at a Mach number of 5.75. The surface heating rates in the stagnation zone of the blunt cone increase by fivefold when the stagnation enthalpy is doubled. The windward corner heating is ~50–60% of the maximum heating rate measured on the blunt cone at 15-deg angle of incidence. The corner bluntness reduces the heat transfer in the corner of the blunt cone by about 10–20%. Slightly higher heating rates are measured in a carbon dioxide environment compared to air as the test gas. These results are used to develop an approximate analytical model for estimating the heating rate distributions over the large-angle blunt cone. The experimental results are also compared with numerical solutions computed using axisymmetric N–S solutions.

References

[1]Raju, I. S., and Craft, W. J., "Analysis and Sizing of Mars Aerobrake Structure," *Journal of Spacecraft and Rockets*, Vol. 30, No. 1, 1993, pp. 102–110.

[2]Scott, C. D., Reid, R. C., Maraia, R. J., Li, C. P., and Derry, S. M., "An AOTV Aero Heating and Thermal Protection Study," AIAA Paper 84-1710, June 1984.

[3]Reddy, N. M., "Heating Rate Measurements Over 30° and 40° (Half Angle) Blunt Cones in Air and Helium in the Langley Expansion Tube Facility," NASA TM-80207, March 1980.

[4]Stewart, D. A., and Chen, Y. K., "Hypersonic Convective Heat Transfer over 140-Degree Blunt Cones in Different Gases," *Journal of Spacecraft and Rockets*, Vol. 31, No. 5, 1994, pp. 735–743.

[5]Hollis, B. R., and Perkins, J. N., "High Enthalpy and Perfect Gas Heating Measurements on a Blunt Cone," *Journal of Spacecraft and Rockets*, Vol. 33, No. 5, 1996, pp. 628–634.

[6]Reddy, N. M., Nagashetty, K., Jagadeesh, G., and Reddy, K. P. J., "Review of Hypersonic Research Investigations in IISc Shock Tunnel (HST-1)," *Sadhana*, Vol. 21, Pt. 6, 1996, pp. 741–773.

[7]Jagadeesh, G., Reddy, N. M., Nagashetty, K., and Reddy, K. P. J., "Forebody Convective Heat Transfer Measurements over Large-Angle Blunt Cones at Hypersonic Mach Number," AIAA Paper 98-2601, June 1998.

[8]Cheng, K. K., Hall, J. G., Golian, T. C., and Hertzberg, A., "Boundary-Layer Displacement and Leading-Edge Bluntness Effects in High Temperature Hypersonic Flow," *Journal of the Aerospace Sciences*, Vol. 28, No. 5, 1961, pp. 353–381.

T. C. Lin
Associate Editor

Aeromaneuvering in the Martian Atmosphere: Simulation-Based Analyses

Roy S. Smith*
University of California, Santa Barbara, Santa Barbara, California 93106
Kenneth D. Mease†
University of California, Irvine, Irvine, California 92697
and
David S. Bayard‡ and David L. Farless§
Jet Propulsion Laboratory, California Institute of Technology, Pasadena, California 91109

Introduction

THE science requirements of future Mars missions include increasing accuracy in the specification of the landing site. In situ science or sample return missions from small craters or ancient lake beds considered to be prime sites for potential exobiology, require a 3-σ target accuracy of 10 km or less.[1] Controlled atmospheric aeromaneuvering will be used to decelerate the vehicle and to guide it to a prespecified terminal point above the surface. At that point a parachute will be deployed to further decelerate the vehicle. An engine will be used for the final controlled descent, from approximately 5 km to the surface.

This Note describes a simulation environment developed to study the guidance, navigation, and control (GNC) aspects of the aeromaneuvering phase. The simulation is modular and based on the widely used MATLAB®/SIMULINK® environment, making it easily upgraded or applied to other landing problems, including landing on other planets or small bodies. A more detailed, and more mission specific, Mars landing simulation is described by Streipe et al.[2] The simulation environment described here is suitable for developing GNC algorithms, investigating the impact of the approach navigation, and performing technology tradeoff studies.

Simulation Environment

The simulation uses a modular approach with each major aspect of the complete system dynamics handled by a separate module. This allows the different aspects of the problem to be developed, upgraded, and modified relatively independently of each other. The major program modules, and conceptual links between each, are illustrated in Fig. 1.

The estimation, guidance, and control aspects have been implemented in separate modules, conforming to historical practice in spacecraft control work. In this problem it is evident that a closer integration of these aspects has the potential for significant performance improvement, and this could be relatively easily done in our simulation.

The environment and spacecraft models are accessed through common modules where flags are used to specify the choice of model, for example, geocentric or geodetic planet models, or even alternative planets. The code for the environment and spacecraft models is linked separately into each module in which it is used. Separate flags are maintained for the simulated physical system models and the GNC models so that effects of knowledge errors may be investigated.

Entry Dynamics

The entry dynamics model used has been derived from the work of Etkin,[3] using the assumption of a rotating planet with its center fixed in inertial space. The vehicle state includes a full six-degree-of-freedom model plus a variable mass (see Ref. 4 for details).

Vehicle Characteristics

Any vehicle model supplying the aerodynamic coefficients, mass properties, and actuator configuration in the correct format can be accomodated. The current vehicle model is based on the Pathfinder entry vehicle (see Refs. 5 and 6 for physical details) augmented with attitude control thrusters and a c.m. offset to generate a lift vector. Eight thrusters are used in the current spacecraft module giving decoupled roll, pitch, and yaw moments.

The aerodynamic model takes into account the effect of the c.m. offset on the pitch and yaw dynamics and allows different nominal lift/drag ratio (L/D) vehicles to be simulated easily. Boussalis[7] describes a longitudinal aerodynamic model, developed from Newtonian impact dynamics, and this forms the basis of the model used in the simulation. The L/D relationship, as a function of angle of attack α is close to linear and can be reasonably approximated by $L/D = -0.0129\alpha$ deg. At $|\alpha| > 20$ deg, the unprotected rear of the vehicle is exposed. Considering $\alpha = -18$ deg as the limit gives a maximum L/D of 0.23.

The roll, pitch, and yaw moment coefficients, C_l, C_m, and C_n, respectively, are modeled by $C_l = 0$, $C_m = C_{\text{moz}} dZ + C_{\text{ma}}\alpha + C_{\text{mq}} q$, and $C_n = -C_{\text{ma}}\beta + C_{\text{nr}} r$, where β is the sideslip angle and q and r are the pitch and yaw rates, respectively. For a nonzero value of the z-axis c.m. offset dZ a nonzero trim value for α (denoted here by α_0) is given by $\alpha_0 = -C_{\text{moz}}/C_{\text{ma}}\, dZ$.

Environmental Models

Atmospheric forces dominate the entry, making the aerodynamic and atmospheric density models more important than the gravity model. In this case a simple spherical planet gravity model is used, $g = \mu/R^2$ m/s^2, where R is the distance from the planet center. Both spherical and geodetic[8] models are available for target and location definition.

The Mars atmospheric density ρ is modeled in exponential form $\rho = \rho_r e^{-\beta(h - h_r)}$, where ρ_r is the reference density $\rho_r = 7.8 \times 10^{-4}$ kg/m^3, specified at an altitude of $h_r = 31.800 \times 10^3$ m. The inverse of the scale height is denoted by β and has a value of $\beta = 10^{-4}$ m^{-1}. A percentage error can be applied to the density to evaluate the effects of density variations on the control system. The modular nature of the simulation environment makes it possible to incorporate a higher fidelity model, for example, Mars Global Reference Atmospheric Model (MarsGRAM) at a later date.

Guidance and Control

The simulation environment supports switching between different guidance algorithms. The focus of the guidance research has been on drag-based predictive tracking algorithms, and two such algorithms (from Refs. 9 and 10) are currently implemented in the simulation.

Drag-tracking algorithms are based on the observation that the predicted range to go is given by integrating a drag/energy profile.

Received 2 April 1999; revision received 6 September 1999; accepted for publication 4 October 1999.

*Associate Professor, Electrical and Computer Engineering. Senior Member AIAA.

†Professor, Mechanical and Aerospace Engineering. Associate Fellow AIAA.

‡Senior Technical Staff, Autonomy and Control. Member AIAA.

§Member Technical Staff, Navigation and Flight Mechanics.